Available online at www.sciencedirect.com

SCIENCE DIRECT®

Journal of the European Ceramic Society 25 (2005) 577–587

www.elsevier.com/locate/jeurceramsoc

Oxidation protection of C/C–SiC composites by an electrophoretically deposited mullite precursor

T. Damjanović[a,*], Chr. Argirusis[a], G. Borchardt[a], H. Leipner[b], R. Herbig[b], G. Tomandl[b], R. Weiss[c]

[a] *Technische Universität Clausthal, Institut für Metallurgie, Robert-Koch-Str. 42, 38678 Clausthal-Zellerfeld, Germany*
[b] *TU Bergakademie Freiberg, Institut für Keramische Werkstoffe, Gustav-Zeuner-Str. 3, 09596 Freiberg, Germany*
[c] *Schunk Kohlenstofftechnik GmbH, Rodheimer Str. 59, 35452 Heuchelheim, Germany*

Received 10 October 2003; received in revised form 22 March 2004; accepted 3 April 2004

Abstract

Electrophoretic deposition (EPD) is a suitable technique to produce mullite layers for acceptable oxidation protection of C/C–SiC composites. Combining sol–gel synthesis of $3Al_2O_3{\cdot}2SiO_2$ mullite through hydrolysis and condensation of tetraethoxysilane (TEOS) and aluminum-tri-*sec*-butylate (Al-$(OBu)_3$) with EPD yields sufficiently thick and homogeneous layers, which transform into mullite at 1300 °C. The protectiveness of the deposited mullite layers was tested in air in the temperature range $1300\,^{\circ}C \le T \le 1550\,^{\circ}C$ by means of isothermal thermogravimetric analysis for up to 200 h. The experimental data can be described by a phenomenological model of the (reduced) oxidation rate of the SiC layer underneath the outer mullite layer, which suggests that transport of carbon monoxide through mullite and silica is rate determining. Comparing the oxidation rate of electrophoretically coated C/C–SiC samples to that of uncoated reference samples clearly demonstrates that mullite offers a significant improvement to the oxidation resistance of the reference material.

Keywords: Mullite; C/C–SiC; Composites; Electrophoretic deposition; Sol–gel processes

1. Introduction

The starting industrial material (Schunk Kohlenstofftechnik GmbH, Heuchelheim, Germany) is a SiC coated carbon-reinforced carbon composite (C/C) in the form of thin slabs with average dimensions 20 mm × 20 mm × 2 mm. The SiC layer is deposited by chemical vapour deposition (CVD) after the C/C substrate has first been capillary infiltrated with liquid silicon. As the CVD process takes place at high temperatures cracks develop in the SiC layer after cooling down to room temperature, which close again after renewed heating above 1100 °C. For short-term oxidation the resulting protective SiO_2 layer is a suitable diffusion barrier but it degrades during prolonged service beyond 1300 °C. Furthermore, silica is not sufficiently resistant against erosion and chemical reactions with other components in the system (e.g., flue ash in power plants or steels in hardening cases for tool production). It is, therefore, necessary to coat the SiC layer with more protective oxides than silica.

Mullite ceramics are promising candidate materials for high temperature applications and oxidation protection of C/C–SiC composites.[1–4] Mullite satisfies all essential requirements for a refractory oxide layer on top of a C/C–SiC composite and has the corresponding mechanical properties: similar low thermal expansion coefficient (average values for CTE of SiC and mullite in the temperature range $20\,^{\circ}C < T < 1000\,^{\circ}C$ are: SiC: $6.1 \times 10^{-6}\,K^{-1}$, mullite: $4.4 \times 10^{-6}\,K^{-1}$), low thermal conductivity, excellent creep resistance, good chemical stability and low oxygen diffusivity.[5,6] Mullite coated SiC exhibits excellent oxidation resistance in dry air by forming a slowly growing native SiO_2 scale under the mullite layer. Depending on the SiO_2 content and on temperature mullite forms a low viscosity grain boundary film which can close cracks and pores, thus offering a certain self-healing capacity.

Plasma spraying or dip coating processes are mostly used to produce mullite layers from mixed oxide or mullite suspensions or from sol–gel systems,[7,8] respectively. The

---

[*] Corresponding author.
E-mail address: tanja.damjanovic@tu-clausthal.de (T. Damjanović).

0955-2219/$ – see front matter © 2004 Elsevier Ltd. All rights reserved.
doi:10.1016/j.jeurceramsoc.2004.04.005

sol–gel synthesis, however, represents a method to prepare ultrapure and nano-sized mullite. Bulk ceramics obtained from powders prepared this way reach nearly theoretical density and have mullitization temperatures below 1500 °C.[9]

This paper demonstrates the possibility to prepare a mullite precursor sol via chemical processing from which electrophoretic deposition (EPD) on C/C–SiC composites produces dense mullite coatings after sintering at 1300 °C, which considerably improve the protectiveness of the primary, SiC coating.

2. Synthesis of the mullite precursor sol

Progress in the synthesis of chemically homogeneous multicomponent oxides is particularly indebted to sol–gel science.[10,11] However, it is well-known that hydrolysis and polycondensation of silicon alkoxides are very slow compared to those of aluminium, and it is difficult to achieve a homogeneous co-polymerization. This may be reached by very slow hydrolysis[12,13] of both alkoxides, by prehydrolysis of the silicon alkoxide,[14] or by modifying the aluminium alkoxide by a chelating group to reduce its reactivity.[15,16]

Reagent grade chemicals used were alkoxides of Si and Al, tetraethoxysilane (TEOS; $C_8H_{20}O_4Si$, VWR International, p.a.) and $Al(OBu)_3$ ($C_{12}H_{27}AlO_3$, VWR International, p.a.), respectively, and isopropyl alcohol (C_3H_7OH, VWR International, p.a.) as a solvent. Due to the pronounced difference in the reactivity of both alkoxides, acetylacetone (AcAc, VWR International, p.a.) was added as a chelating agent inhibiting the condensation of $Al(OBu)_3$. TEOS as a slower reacting precursor was prehydrolyzed with water of different pH values (pH 2, 6, 10) adjusted by the addition of hydrochloric acid and ammonia.

For the synthesis of suitable mullite precursors the concentration of the separate alkoxide solutions, the pH of water (pH 2, 6, 10), the molar ratio of the water to TEOS ($r_W =$ 2–10) and the concentration of acetylacetone were varied (0.01–1 M) in order to obtain a series of different mullite precursor sols, whose electrokinetic properties were to be investigated systematically later on.

The synthesis of $Al(OBu)_3$–isopropanol solution was performed in a glove box so as to avoid uncontrollable atmospheric moisture. $Al(OBu)_3$ was dissolved in isopropyl alcohol on stirring, and acetylacetone was added into the $Al(OBu)_3$ solution until a final concentration 0.1 M was reached. In the meantime, the separate solution of TEOS was prepared. This reaction was performed in air because of the lower reactivity of the Si alkoxide. TEOS was prehydrolyzed for 1 h by addition of water of defined pH. The addition of water was controlled by an automatic titrator (736 GP Titrino, Metrohm, Germany). The interval of titration was 10 s and the flow rate was 2 ml min^{-1}.

The final mullite precursor sol was obtained under controlled addition of the $Al(OBu)_3$ solution to the TEOS sol in a ratio corresponding to stoichiometric mullite ($3Al_2O_3 \cdot 2SiO_2$). Final mixing of both sols was performed in air with the $Al(OBu)_3$ sol covered with a parafilm to avoid additional hydrolysis by atmospheric moisture. According to the mullite composition, a larger volume of $Al(OBu)_3$ solution had to be mixed with a smaller volume of the TEOS solution. It would be technically easier to add the TEOS solution to the $Al(OBu)_3$ solution but this sequence leads to higher local concentrations of Al and induces inhomogeneities and phase separation in the final sol. Due to this fact, the $Al(OBu)_3$ solution was added in small volume increments to the TEOS solution. The addition was performed in volume increments of 0.1 ml, with a flow rate of 1 ml min^{-1} in intervals of 10 s, by an automatic titrator. The TEOS sol was stirred during the addition of the $Al(OBu)_3$ solution, and the whole experiment was performed at room temperature.

From the systematic investigations to optimize the above mentioned parameters of the sol–gel synthesis (concentration of alkoxide solutions, pH value, amount of water needed for prehydrolysis of TEOS and amount of chelating agent), two promising experimental procedures were identified:

(i) Synthesis of a mullite precursor sol was possible under the following conditions: concentration of alkoxide–isopropanol solutions is 10 vol.%, pH 7 (distilled water), $r_W = 2$, addition of acetylacetone ($c =$ 0.1 M). This precursor will be further denoted as MP1 in the text.

(ii) Synthesis of a mullite precursor sol with alkoxide–isopropanol solutions of 10 vol.%, pH 2 (adjusted by addition of HCl), $r_W = 10$ and addition of acetylacetone ($c = 0.1$ M). Due to the higher amount of water added for the hydrolysis of TEOS and prolonged co-polymerization of both alkoxides, we obtained a particulate sol suitable for the electrophoretic deposition of the mullite precursor. This precursor will be further denoted as MP2 in the text.

3. Characterization of the mullite precursors

The characterization of the stability and the mobility of the two mullite precursors prepared as described in Section 2, was carried out by electrokinetic sonic analysis (ESA-8000, MATEC Applied Sciences, USA). The average particle size of the synthesized mullite precursors MP1 ($d_{50} \approx 20$ nm) and MP2 ($d_{50} \leq 50$ nm), was estimated by means of transmission electron microscopy (TEM). The ESA measurements gave an ESA amplitude of 7.80 μPa m V^{-1} (corresponding to a zeta-potential value of $\zeta = 5.2$ mV) for the mullite precursor MP1 and of 22.59 μPa m V^{-1} ($\zeta = 15.1$ mV) for the mullite precursor MP2. Because of its low conductivity MP1 was not suitable for the electrophoretic deposition, in contrast to MP2.

In order to get information about the thermal behaviour of the precursors, as well as to determine structural changes as a function of the annealing regimes, XRD (Siemens D5000 diffractometer), DTA/TG (Shimadzu Thermal Analyzer) and ^{29}Si and ^{27}Al MAS NMR (Bruker MSL 300 MHz spectrometer) studies were performed.

For the mullite precursor MP1 the DTA/TG peak at 996.5 °C corresponded to mullite formation which was confirmed by means of XRD analysis. This means that the obtained precursor sol was a single phase with both alkoxides mixed on a molecular scale leading to mullite crystallization at $T \leq 1000\,^\circ\mathrm{C}$.

For the mullite precursor MP2, XRD investigations showed that the precursor remains amorphous up to approximately 1000 °C. The DTA/TG peak at 1129 °C corresponds to the formation of an alumina spinel also confirmed by XRD. After a heat treatment at 1250 °C, according to XRD phase analysis, crystalline mullite is formed. According to the literature[16] higher mullitization temperatures ($T \geq 1250\,^\circ\mathrm{C}$) indicate that the synthesized mullite precursor MP2 is diphasic already in the sol state.

These conclusions on the homogeneity of the synthesized mullite precursors were confirmed by means of NMR analysis. The NMR results on the two different mullite precursors described above can explain the different mullitization temperatures. The detected chemical shifts and the respective signal assignments[17] are given in Table 1.

For a homogeneous mullite precursor a mullite-like Si surrounding, i.e., Si(4Al) units should be present in the NMR spectra. The preliminary stage of the mullite precursor MP1 (heat-treated at 550 °C) and the finally formed sol–gel mullite from MP1 at 1300 °C fulfil this expectation, whereas the non-crystalline phase from the mullite precursor MP2 at 550 °C causes a broad signal in the spectrum. The peak maxima for both thermal stages of MP1 (Fig. 1a and c) are in the region for Si(4Al). The spectrum of the MP2 precursor at 550 °C (Fig. 1b) shows significant evidence for silicon surrounded by less than four OAl groups, which triggers the formation of SiO_2 rich and SiO_2 deficient domains in the annealed precursor. This finally results in higher mullitization temperatures than for the (more homogeneous) precursor MP1.

Numerous ^{27}Al NMR studies of aluminium-containing amorphous xerogels of oxide glasses have revealed the presence of three different aluminium environments.[18] Aluminium nuclei in octahedral and tetrahedral environments give rise to characteristic chemical shifts of 0 and 60 ppm, respectively. The third species at 30 ppm has been attributed to an [AlO_5] environment because its chemical shift lies between those of [AlO_6] and [AlO_4] and is very similar to the signal observed in well-known pentacoordinated Al compounds. Recently, it has been suggested by Schmücker and Schneider[19] that in Al_2O_3-rich aluminium silicate gels and glasses with compositions close to mullite, this signal may arise from some tricluster [AlO_4] units.

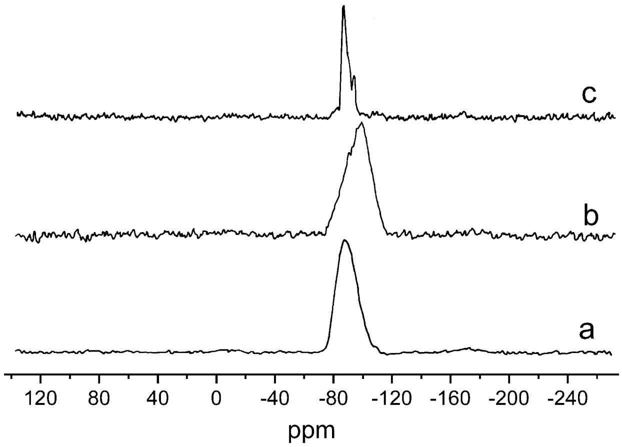

Fig. 1. ^{29}Si solid state NMR: (a) CP/MAS spectrum of the preliminary stage of MP1 (550 °C), (b) CP/MAS spectrum of MP2 (550 °C) and (c) CP/MAS spectrum of MP1 (1300 °C).

Taylor and Holland[20] have related the aluminium coordination in aluminosilicate gels to their homogeneity, suggesting that Al(4) sites exist in regions of uniform Al/Si dispersion and reflect the efficient incorporation of aluminium into the tetrahedral silicate network. Less homogeneous regions containing discrete alumina-rich and silica-rich domains are believed to result in an increased proportion of Al(6) sites. By comparing the values of the composite quadrupolar coupling constant and of the isotropic chemical shift for the intermediate peaks in a mullite glass precursor and in crystalline mullite Bodart et al.[18] confirmed that metastable aluminium atoms are present in the mullite glass precursor in an essentially pentacoordinated environment. Jaymes et al.[21] also suggested that the concentration of hexacoordinated Al atoms in single phase precursors practically completely disappears before mullite crystallization at 980 °C. In diphasic precursors the aluminosilicate phase

Table 1
Results of ^{29}Si and ^{27}Al solid state NMR measurements

Sample	^{29}Si MAS or CP/MAS NMR[21] chemical shift (ppm)	Assignment of ^{29}Si chemical shifts	^{27}Al SATRAS NMR[22] chemical shift (ppm)	Assignment of ^{27}Al chemical shifts
MP2 (550 °C)	−75 to –115 (max. –99.2)	Si(2Al)	3.4	CN 6 ≫ CN 4 (shoulder), CN 5 present
MP1 (550 °C)	−70 to –112 (max. –87.6)	Si(4Al)	26.1, 2.0	CN 5 strongest signal CN 6 ≫ CN 4
MP1 (1300 °C)	−86.1, shoulder –89, −93.3	Si(3Al), Si(4Al)	42.4, 1.9	CN 6∼CN 4, CN 4 shoulder

^{29}Si NMR measuring conditions: MSL 300 MHz, Larmor frequency 59.627 MHz, CP time 5 ms; ^{27}Al NMR measuring conditions: MSL 300 MHz, Larmor frequency 78.205 MHz. CN: co-ordination number of Al; CP/MAS NMR: cross polarization/magic angle spinning NMR spectroscopy; SATRAS NMR: satellite transition NMR spectroscopy.

has a higher content in AlO_6 octahedra, resulting in the crystallization of a spinel phase.

The ^{27}Al NMR spectra[22] of the preliminary stage of the mullite precursor MP1, the mullite obtained from the precursor MP1 after heating to 1300 °C and the mullite precursor MP2 show three Al signals assigned to different co-ordination numbers (CN) for each sample (Table 1). From the results presented in Table 1 it is obvious that the mullite precursor MP2 which is suitable for EPD has in its amorphous structure at 550 °C a high concentration of hexacoordinated Al atoms. These Al(6) sites exist as a result of inhomogeneties at the Al–Si mixing scale and, according to this, MP2 crystallizes into mullite at temperatures only above 1250 °C. On the other hand, the mullite precursor MP1 at 550 °C has the strongest NMR signal for pentacoordinated aluminium which according to Schmücker and Schneider[19] acts as mullite nucleus because of a locally decreased activation energy. This precursor crystallizes directly into mullite below 1000 °C without formation of spinel, but is unfortunately unsuitable for electrophoretic deposition, as mentioned above.

4. EPD of mullite from the precursor sol

As the uniformity of the deposited layer is strongly dependent on the homogeneity of the surrounding electrical field,[23,24] the following experimental set-up for EPD was chosen (Fig. 2):

- The substrate (C/C–SiC composite) was placed vertically in the mullite precursor sol with its surface parallel to the counter electrodes made of stainless steel.
- Both the substrate and the counter electrodes were of planar geometry.
- The distance between the counter electrodes and the substrate was kept fixed at 10 mm.
- The surface of the counter electrodes (40 mm × 60 mm) was larger than the surface of the substrate (20 mm × 20 mm), which yields a reasonably uniform electrical field near the substrate.
- In order to avoid electrode marks on the substrate the position of the point contacts was changed before each individual deposition step.

The topography of the sample surface was investigated with a surface profiler (Alpha-Step 500, Tencor). The roughness of the surface[25] is characterized by the following parameters: the average roughness, Ra = 3.71 μm, and the maximum peak-valley amplitude called total indicator run-out, TIR = 50.02 μm.

As explained above only the precursor MP2 was suitable for our purposes and EPD was performed cathodically with different voltages and durations of deposition. The best performance of the deposited layer regarding the adhesion of the green layer to the C/C–SiC substrate after drying, was achieved with 15 V cm^{-1} and 15 and 30 s deposition time. Under these conditions the deposited mass is directly proportional to the deposition time. The average mass gain per deposition cycle at 15 V cm^{-1} and 15 or 30 s was 0.16 and 0.37 mg cm^{-2}, respectively. All C/C–SiC substrates were coated five-times with a sintering step between each deposition step at 1300 °C (mullitization temperature obtained from XRD investigations on the mullite precursor MP2) in an atmosphere of 99.996% Ar for 2 h. After the final sintering step the deposited layers were investigated by means of secondary electron microscopy (SEM) in order to obtain information about the thickness of the deposited layer and its composition.

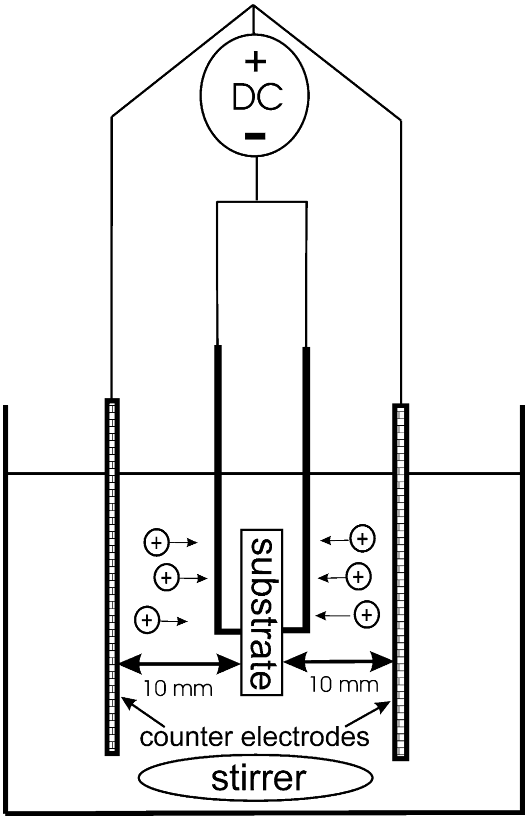

Fig. 2. Experimental set-up for EPD of the mullite precursor.

On the presented SEM micrograph (Fig. 3) the deposited mullite layer is shown for the EPD conditions of 15 V/15 s. According to the SEM micrograph, it is obvious that for the chosen EPD conditions the obtained layer adheres well to the surface of the substrate. The EDX analysis at the indicated spot showed a composition close to 3/2-mullite.

5. Thermogravimetric analysis of the oxidation rate in air

The protectiveness of the electrophoretically deposited mullite layers against isothermal oxidation in air in the temperature range from 1300 to 1550 °C was investigated by

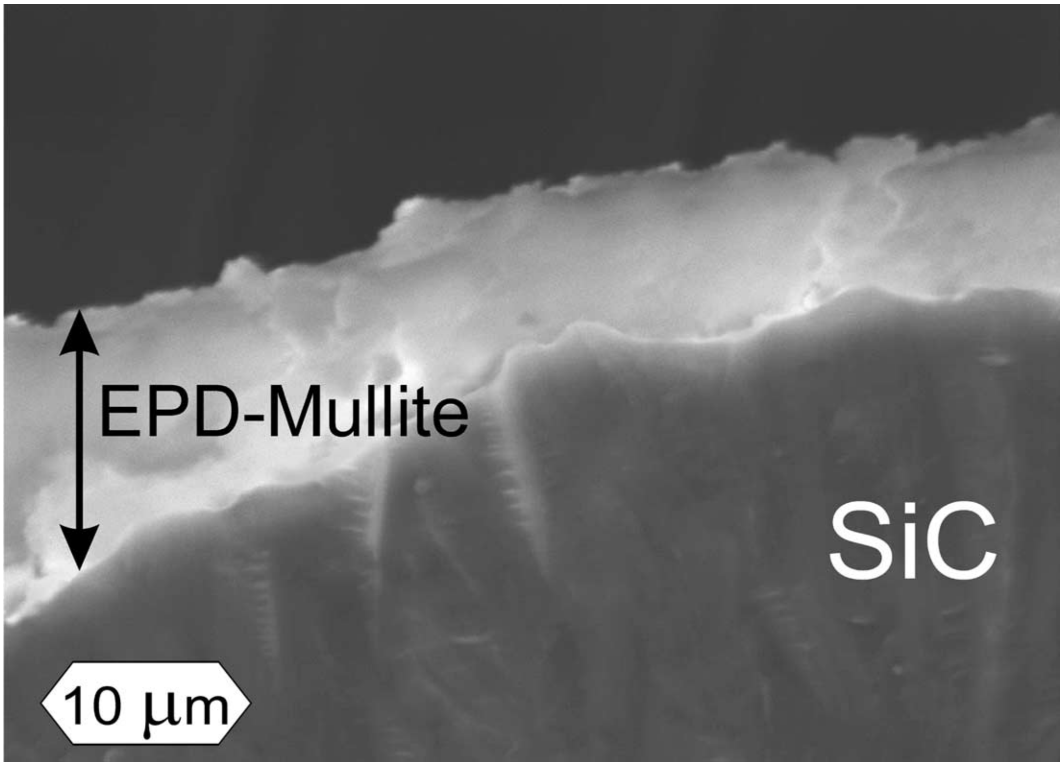

Fig. 3. SEM micrograph of the cross-section of the electrophoretically deposited mullite layer on C/C–SiC at 15 V cm^{-1} for 15 s (1×: EDX analysis spot).

means of thermogravimetry (TG). The results are given in Table 2.

The experimentally obtained values for the oxidation rate of the mullite coated C/C–SiC samples were interpreted with the help of a phenomenological model whose basic version had been originally developed in our group by Fritze et al.[1] for pulsed laser deposited mullite layers. According to this model (see Fig. 4a), the samples exhibit a mass gain in the whole temperature range, due to the passive oxidation of the SiC layer. The formation of SiO_2 overcompensates the mass loss due to CO formation according to the reaction:

$$SiC + \frac{3}{2}O_2 \rightarrow SiO_2 + CO \qquad (1)$$

The model will be applied to two situations, named case A and case B in the following.

Table 2
Practical linear rate constants, k'_L, and practical parabolic rate constants, k'_p, for $T \leq 1350\,^\circ C$ and for $T \geq 1400\,^\circ C$. The experimental values were, respectively, determined with the help of Eqs. (14) and (16)

T (°C)	k'_L (mg cm^{-2} h^{-1})	k'_{0L} (mg cm^{-2} h^{-1})	ΔH_a (kJ mol^{-1})
1300	1.72×10^{-3}	1.53×10^{8}	330
1350	3.74×10^{-3}		
	k'_p (mg^2 cm^{-4} h^{-1})	k'_{0P} (mg cm^{-4} h^{-1})	
1400	4.91×10^{-5}	1.12×10^{7}	362 ± 66
1450	1.61×10^{-4}		
1500	1.90×10^{-4}		
1550	5.00×10^{-4}		

Case A: The rate-limiting step is assumed to be transport of oxygen through the protective layer composed of the mullite layer and a native SiO_2 layer growing underneath. Under the assumption that mullite does not substantially dissolve in the silica scale, the time (t) dependent thickness of the growing SiO_2 layer, $x_S(t)$, is obtained as follows:[1]

With the atomic or ionic oxygen flux densities j_M and j_S in the mullite (M) and in the silica layer (S), respectively,

$$j_M = -\frac{\tilde{D}_M c_M}{RT}\left(\frac{\partial \mu_O}{\partial x_M}\right) \qquad (2a)$$

$$j_S = -\frac{\tilde{D}_S c_S}{RT}\left(\frac{\partial \mu_O}{\partial x_S}\right) \qquad (2b)$$

the formal molecular flux density, j_{O_2}, of oxygen can be derived as follows:

$$j_{O_2} = \frac{1}{2} j_M = \frac{1}{2} j_S = \frac{1}{4}\frac{\tilde{D}_S c_S \tilde{D}_M c_M}{\tilde{D}_S c_S x_M + \tilde{D}_M c_M x_S}\frac{|\Delta \mu_{O_2}|}{RT} \qquad (3)$$

where $\tilde{D}_S$, $\tilde{D}_M$ is the effective chemical diffusivity of oxygen O, (O^{2-} or O_2), in vitreous (or polycrystalline) SiO_2 and in polycrystalline mullite; $x_S(t)$, x_M is the thickness of the silica layer and of the mullite layer; c_S, c_M is the molar concentration of oxygen in silica and in crystalline 3/2-mullite; μ_O is the chemical potential of oxygen ($= 1/2\mu_{O_2}$); $\Delta\mu_{O_2}$ is the difference of the chemical potential of oxygen (see Fig. 4a: $\mu_{O_2}(\mathrm{I}) - \mu_{O_2}(\mathrm{III})$).

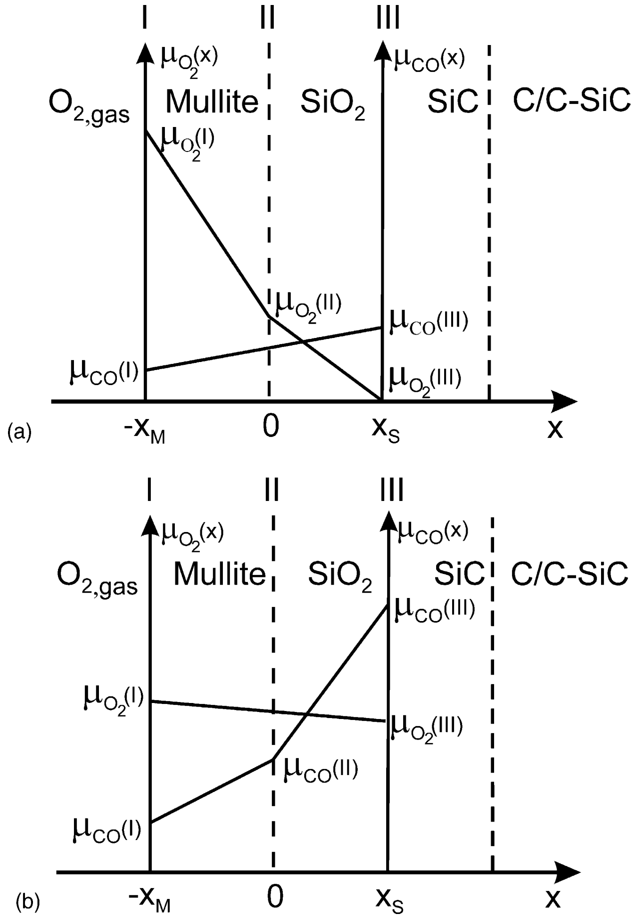

Fig. 4. (a and b) Schematic representation of the variation of the chemical potential of O_2 and CO in the layer system mullite-SiO_2 according to the case A (oxygen diffusion rate determining) and case B (CO diffusion rate determining), respectively.

According to Eq. (1) the growth rate of the silica layer at the interface III is given by the following expression:

$$\frac{dx_S(t)}{dt} = \frac{2}{3} V_{m,SiO_2} j_{O_2} \tag{4}$$

which, together with Eq. (3), yields after integration:

$$x_S(t) = \alpha\left(\sqrt{(1+\beta t)} - 1\right) \tag{5}$$

where the parameters α and β are defined as follows:

$$\alpha = \frac{2}{13}\frac{V_{m,M}}{V_{m,S}}\frac{\tilde{D}_S}{\tilde{D}_M} x_M$$

$$\beta = \frac{169}{6}\left(\frac{V_{m,S}}{V_{m,M}}\right)^2 \frac{|\Delta\mu_{O_2}|}{RT}\frac{1}{x_M^2}\frac{\tilde{D}_M^2}{\tilde{D}_S} \tag{7}$$

where $V_{m,S}$, $V_{m,M}$ is the molar volume of silica and of mullite, respectively.

As long as the growing SiO_2 layer is much thinner than the deposited mullite layer (short oxidation times, i.e., $\beta t \ll 1$), oxygen diffusion through the mullite layer is the rate limiting step and the oxidation kinetics is linear. Eq. (5) reduces to:

$$x_S(t) = \frac{1}{2}\alpha\beta t = \frac{13}{6}\frac{V_{m,S}}{V_{m,M}}\frac{|\Delta\mu_{O_2}|}{RT}\frac{\tilde{D}_M}{x_M} t = k_L t \tag{8}$$

with

$$k_L = \frac{13}{6}\frac{V_{m,S}}{V_{m,M}}\frac{|\Delta\mu_{O_2}|}{RT}\frac{\tilde{D}_M}{x_M} \tag{9}$$

as the linear rate constant, which is directly proportional to the oxygen diffusion coefficient in the mullite layer, $\tilde{D}_M$, and inversely proportional to the thickness of the mullite layer, x_M.

Longer oxidation times ($\beta t \gg 1$) lead to thicker SiO_2 layers, and transition from the linear to the parabolic growth law will occur:

$$x_S(t) = \alpha\beta^{1/2}t^{1/2} = \left(\frac{2}{3}\frac{|\Delta\mu_{O_2}|}{RT}\tilde{D}_S\right)^{1/2} t^{1/2} = \sqrt{2k_P}\sqrt{t} \tag{10}$$

The parabolic rate constant k_P is defined as:

$$k_P = \frac{1}{2}\alpha^2\beta = \frac{1}{3}\frac{|\Delta\mu_{O_2}|}{RT}\tilde{D}_S \tag{11}$$

and is directly proportional to the oxygen diffusion coefficient in the SiO_2 layer, $\tilde{D}_S$. In agreement with the experiments this simple model shows that after long times the oxidation kinetics become parabolic.

For the evaluation of the TG data, the oxidation rate can be expressed in terms of the mass change rate:

$$\frac{1}{A_0}\frac{d(\Delta m_{sample})}{dt} = \frac{\rho_S}{3}\frac{dx_S}{dt} = \frac{\rho_S}{6}\frac{\alpha\beta}{\sqrt{1+\beta t}} \tag{12}$$

where A_0 is the total (geometrical) surface of the sample, ρ_S the density of amorphous silica or β-cristobalite, respectively.

For short oxidation times ($\beta t \ll 1$) Eq. (12) yields a constant oxidation rate:

$$\frac{1}{A_0}\frac{d(\Delta m_{sample})}{dt} = \frac{\rho_S}{6}\alpha\beta = k'_L \tag{13}$$

which, after integration, yields a linear time dependency for the mass change:

$$\frac{\Delta m_{sample}}{A_0} = k'_L t \tag{14}$$

with k'_L as a practical linear rate constant (for TG experiments).

For longer oxidation times ($\beta t \gg 1$) we obtain from Eq. (12) a time dependent oxidation rate:

$$\frac{1}{A_0}\frac{d(\Delta m_{sample})}{dt} = \frac{\rho_S}{6}\alpha\frac{\sqrt{\beta}}{\sqrt{t}} = \sqrt{\frac{k'_P}{2t}} \tag{15}$$

which, after integration, yields a parabolic time dependency for the mass change:

$$\left(\frac{\Delta m_{sample}}{A_0}\right)^2 = 2k'_P t \tag{16}$$

Table 3
Calculated rate constants

T (°C)	k'_{L} ($mg\,cm^{-2}\,h^{-1}$)	k'_{0L} ($mg\,cm^{-2}\,h^{-1}$)	ΔH_a ($kJ\,mol^{-1}$)
1300	1.85×10^{-1}	1.38×10^{11}	357
1350	4.30×10^{-1}		
k'_{P} from Eq. (18) with $\tilde{D}_S$ from Eq. (19) after Rodriguez-Viejo et al.[27]: vitreous SiO_2			
	k'_{P} ($mg^2\,cm^{-4}\,h^{-1}$)	k'_{0P} ($mg^2\,cm^{-4}\,h^{-1}$)	
1400	1.05×10^{-2}	7.37×10^{7}	315
1450	2.03×10^{-2}		
1500	3.78×10^{-2}		
1550	6.78×10^{-2}		
k'_{P} from Eq. (18) with $\tilde{D}_S$ from Eq. (20) after Rodriguez-Viejo et al.[27]: β-cristobalite			
	k'_{P} ($mg^2\,cm^{-4}\,h^{-1}$)	k'_{0P} ($mg^2\,cm^{-4}\,h^{-1}$)	
1400	2.80×10^{-3}	4.0×10^{10}	421
1450	6.74×10^{-3}		
1500	1.54×10^{-2}		
1550	3.38×10^{-2}		

Case A: Oxygen diffusion rate determining; k'_L from Eq. (17) with $\tilde{D}_{\mathrm{Meff}}$ from Eq. (24) after Fielitz et al.[5,6,26]

with k'_P as a practical parabolic rate constant (for TG experiments).

With the working Eqs. (17) and (18):

$$k'_L = \frac{13}{18}\frac{M_S}{V_{m,M}}\frac{|\Delta\mu_{O_2}|}{RT}\frac{\tilde{D}_M}{x_M} = \frac{\rho_S}{3}k_L \qquad (17)$$

$$k'_P = \frac{\rho_S^2}{9}\frac{1}{3}\frac{|\Delta\mu_{O_2}|}{RT}\tilde{D}_S = \frac{\rho_S^2}{9}k_P \qquad (18)$$

oxidation rate constants can be calculated from diffusivity data for the linear and for the parabolic growth regime, respectively, and can be compared with experimentally obtained values (see Tables 2 and 3) depending on the given oxidation time and temperature. For the molar volume of mullite and for the densities of the vitreous silica and of β-cristobalite, respectively, the following values were adopted: $V_{m,M} = 134.81\,cm^3\,mol^{-1}$, $\rho_{am} = 2.2\,g\,cm^{-3}$, $\rho_{cr} = 2.27\,g\,cm^{-3}$, $M_S = 60.082\,g\,mol^{-1}$ is the molar mass of SiO_2.

The thickness of the EPD–mullite layer was $x_M = 7.5\,\mu m$ (for EPD at 15 V/15 s).

For the diffusion data for oxygen in single crystalline 2/1-mullite[5] and polycrystalline 3/2-mullite,[6,26] in amorphous silica and in β-cristobalite,[27] respectively, the following data set was used:

SiO_2: see Rodriguez-Viejo et al.[27]

$$D_{am} = 1.1 \times 10^{-6}\exp\left(-\frac{333\,kJ\,mol^{-1}}{RT}\right)\ (m^2\,s^{-1}) \qquad (19)$$

$$D_{cr} = 5.6 \times 10^{-4}\exp\left(-\frac{439\,kJ\,mol^{-1}}{RT}\right)\ (m^2\,s^{-1}) \qquad (20)$$

Mullite: see Fielitz et al.[5,6,26]

$$D_V = 3.71 \times 10^{-5}\exp\left(\frac{-(433 \pm 21)kJ\,mol^{-1}}{RT}\right)\ (m^2\,s^{-1}) \qquad (21)$$

$$D_{GB} = 6.2 \times 10^{-3}\exp\left(\frac{-(363 \pm 25)\,kJ\,mol^{-1}}{RT}\right)\ (m^2\,s^{-1}) \qquad (22)$$

As has been shown,[5] there is only a small difference in the bulk diffusivity, D_V, measured in 2/1-mullite and in 3/2-mullite.

For our calculations, we used an effective tracer diffusivity, D_{Meff}, for the oxygen transport in polycrystalline mullite:

$$D_{\mathrm{Meff}} = D_V\left(1 + \frac{4\delta}{d}\frac{D_{GB}}{D_V}\right) \qquad (23)$$

where $\delta \approx 1\,nm$ is the grain boundary thickness and $d \approx 35\,nm$ is the grain size, which was determined from XRD peak broadening.

Inserting the values for δ and d in Eq. (23) together with the data for volume and grain boundary tracer diffusion of oxygen in polycrystalline mullite, we get the following expression for D_{Meff}:

$$D_{\mathrm{Meff}} = 3.7 \times 10^{-5}\,e^{-(433\pm21)\,kJ\,mol^{-1}/RT} \times (1 + 19.1\,e^{(70\pm46)kJ\,mol^{-1}/RT})\ (m^2\,s^{-1}) \qquad (24)$$

i.e., D_{Meff} (1573 K) $\approx 4 \times 10^3 D_V$ (1573 K).

The calculated values of k'_L and k'_P given in Table 3 were obtained by setting $\tilde{D}_S = D_{am}$ (from Eq. (19)) or $\tilde{D}_S = D_{cr}$ (from Eq. (20)) and $\tilde{D}_M = D_{\mathrm{Meff}}$ (from Eq. (24)).

The value of $\Delta\mu_{O_2}$ is estimated as follows: the standard Gibbs energy of formation for the reaction in Eq. (1), ΔG_1°, can be expressed by the corresponding standard Gibbs energies of formation for SiO_2, SiC and CO[28]:

$$\Delta G_1^\circ = \Delta G_{SiO_2}^\circ - \Delta G_{SiC}^\circ + \Delta G_{CO}^\circ \qquad (25)$$

The equilibrium condition at the SiO_2/SiC interface (III) leads to:

$$e^{-\Delta G_1^\circ/RT} = \frac{a_{CO}\,(III)}{a_{O_2}^{3/2}\,(III)} \qquad (26)$$

with a_{CO}, a_{O_2} being the activities of CO and O_2, respectively.

In general, a_{CO} (III) will be lower than unity. If, for the sake of simplicity, we set a_{CO} (III) = 1, we obtain:

$$a_{O_2}(III) = (e^{\Delta G_1^\circ(T)/RT})^{2/3} \qquad (27)$$

i.e.,

$$\frac{\Delta\mu_{O_2}}{RT} = \ln 0.2 - \frac{2}{3}\frac{\Delta G_1^\circ}{RT} \qquad (28)$$

for oxidation in air ($a_{O_2}(I) = 0.2$).

In the temperature range under study, $1573\,K \le T \le 1823\,K$, $\Delta\mu_{O_2}/RT$ varies between 39.84 and 33.32.

As can be seen from Tables 2 and 3, respectively, the experimental values for both k'_L and k'_P are at least one order of magnitude lower than the calculated ones if oxygen transport through amorphous silica or cristobalite is assumed to be the rate determining step.

Case B: Instead of oxygen inward diffusion the outward diffusion of CO and/or an interface reaction could be the rate limiting steps. For the case of oxidation of uncoated SiC this possibility has been already briefly discussed some time ago by Luthra.[29,30]

In analogy to the derivation given for case A above, the growth rate of the native silica scale underneath the outer mullite layer is now given by the following expression:

$$\frac{\mathrm{d}x_\mathrm{S}}{\mathrm{d}t} = j_\mathrm{CO} V_\mathrm{m,S} = V_\mathrm{m,S} \frac{|\Delta\mu_\mathrm{CO}|/RT}{x_\mathrm{S}/\tilde{D}^*_\mathrm{S} c^*_\mathrm{S} + x_\mathrm{M}/\tilde{D}^*_\mathrm{M} c^*_\mathrm{M} + 1/k_\mathrm{III}} \tag{29}$$

where $k_\mathrm{III} = j_\mathrm{CO}(\mathrm{III})/(|\Delta\mu_\mathrm{CO}(\mathrm{III})|/RT)$ is the reaction rate constant at the interface III (see Fig. 4b), and the superscript $*$ means that the diffusivities and solubilities now refer to CO, whose total chemical potential difference, $\Delta\mu_\mathrm{CO}$, is given by $\Delta\mu_\mathrm{CO} = \mu_\mathrm{CO}\,(\mathrm{III},\ \mathrm{max}) - \mu_\mathrm{CO}(\mathrm{I})$.

After integration, Eq. (29) yields again Eq. (5), but now with

$$\alpha = \tilde{D}^*_\mathrm{S} c^*_\mathrm{S} \left(\frac{x_\mathrm{M}}{\tilde{D}^*_\mathrm{M} c^*_\mathrm{M}} + \frac{1}{k_\mathrm{III}} \right) \tag{30}$$

$$\beta = \frac{2V_\mathrm{m,S}}{\tilde{D}^*_\mathrm{S} c^*_\mathrm{S}} \left(\frac{\tilde{D}^*_\mathrm{M} c^*_\mathrm{M} k_\mathrm{III}}{\tilde{D}^*_\mathrm{M} c^*_\mathrm{M} + x_\mathrm{M} k_\mathrm{III}} \right)^2 \frac{|\Delta\mu_\mathrm{CO}|}{RT} \tag{31}$$

The corresponding practical linear rate constant (for TG experiments) now reads:

$$k'^*_\mathrm{L} = \frac{M_\mathrm{S}}{3} \frac{|\Delta\mu_\mathrm{CO}|}{RT} \frac{(\tilde{D}^*_\mathrm{M} c^*_\mathrm{M}/x_\mathrm{M}) k_\mathrm{III}}{\tilde{D}^*_\mathrm{M} c^*_\mathrm{M}/x_\mathrm{M} + k_\mathrm{III}} \tag{32}$$

which becomes

$$k'^*_\mathrm{L} = \frac{M_\mathrm{S}}{3} \frac{|\Delta\mu_\mathrm{CO}|}{RT} k_\mathrm{III} \quad \text{for} \quad \frac{\tilde{D}^*_\mathrm{M} c^*_\mathrm{M}}{x_\mathrm{M}} \gg k_\mathrm{III} \tag{33}$$

and

$$k'^*_\mathrm{L} = \frac{M_\mathrm{S}}{3} \frac{|\Delta\mu_\mathrm{CO}|}{RT} \frac{\tilde{D}^*_\mathrm{M} c^*_\mathrm{M}}{x_\mathrm{M}} \quad \text{for} \quad \frac{\tilde{D}^*_\mathrm{M} c^*_\mathrm{M}}{x_\mathrm{M}} \ll k_\mathrm{III} \tag{34}$$

respectively.

Likewise, we get for the practical parabolic rate constant (for TG experiments):

$$k^*_\mathrm{P} = \frac{\rho_\mathrm{S}}{9} M_\mathrm{S} \frac{|\Delta\mu_\mathrm{CO}|}{RT} \tilde{D}^*_\mathrm{S} c^*_\mathrm{S} \tag{35}$$

Up to now, neither diffusivities nor solubilities for CO in silica and in mullite are available from the literature. Assuming CO molecules to be the diffusing species, the permeation parameter $\tilde{D}^*_\mathrm{i} c^*_\mathrm{i}$ (i = S, M) should be fairly similar in silica and mullite. We, therefore, first calculate $\tilde{D}^*_\mathrm{S} c^*_\mathrm{S}$ for silica from Eq. (35). With

$$\frac{\Delta\mu_\mathrm{CO}}{RT} = \ln a_\mathrm{CO}\,(\mathrm{III}) - \ln a_\mathrm{CO}\,(\mathrm{I}) \tag{36}$$

we get for $10^{-5} \le a_\mathrm{CO}(\mathrm{I}) \le 10^{-4}$ and $a_\mathrm{CO}(\mathrm{III}) \simeq 1$ (see Luthra[29] and Fig. 4b) $|\Delta\mu_\mathrm{CO}/RT| \approx 10$.

With our experimental parabolic rate constant:

$$k'_\mathrm{P} = 1.12 \times 10^7 \exp\left(-\frac{(362 \pm 66)\,\mathrm{kJ\,mol^{-1}}}{RT} \right) \times (\mathrm{mg^2\,cm^{-4}\,h^{-1}}) \tag{37}$$

we obtain:

$$\tilde{D}^*_\mathrm{S} c^*_\mathrm{S} = 2.12 \times 10^{-5} \exp\left(-\frac{(362 \pm 66)\,\mathrm{kJ\,mol^{-1}}}{RT} \right) \times (\mathrm{mol\,cm^{-1}\,s^{-1}}) \tag{38}$$

On the other hand, Eq. (34) yields for $x_\mathrm{M} = 7.5\,\mu\mathrm{m}$

$$\tilde{D}^*_\mathrm{M} c^*_\mathrm{M} = 1.59 \times 10^{-4} \exp\left(-\frac{330\,\mathrm{kJ\,mol^{-1}}}{RT} \right) \times (\mathrm{mol\,cm^{-1}\,s^{-1}}) \tag{39}$$

from our experimental linear rate constant k'_L:

$$k'_\mathrm{L} = 1.53 \times 10^8 \exp\left(-\frac{330\,\mathrm{kJ\,mol^{-1}}}{RT} \right) (\mathrm{mg\,cm^{-2}\,h^{-1}}) \tag{40}$$

The ratio of the permeation parameters of silica and mullite, $\tilde{D}^*_\mathrm{S} c^*_\mathrm{S}/\tilde{D}^*_\mathrm{M} c^*_\mathrm{M} = 0.13 \exp((-(32 \pm 66)\,\mathrm{kJ\,mol^{-1}})/RT)$, yields ≈0.1, as the exponential term is practically unity because of the error in the exponent.

The occurrence of a rate determining interface reaction (most probably at the interface III between SiO_2 and SiC) must be discarded as the respective rate constant which can be calculated with Eq. (33) would have an unreasonably low value (confer Luthra[31]).

6. Discussion

The evaluation of the isothermal TG data shows that the oxidation kinetics are indeed linear below 1350 °C and parabolic above this temperature (at least for test durations of less than about 200 h, see Figs. 5 and 6).

From the Arrhenius diagram (Fig. 7) an effective activation enthalpy for k'_P, $\Delta H_\mathrm{a} = (362 \pm 66)\,\mathrm{kJ\,mol^{-1}}$, has been calculated for the temperature interval $1400\,^\circ\mathrm{C} < T < 1550\,^\circ\mathrm{C}$. Within the parabolic regime the oxidation rate should be controlled by solid state diffusion processes in the growing native silica scale. As can be seen from Table 3 oxygen transport in either amorphous or crystalline silica

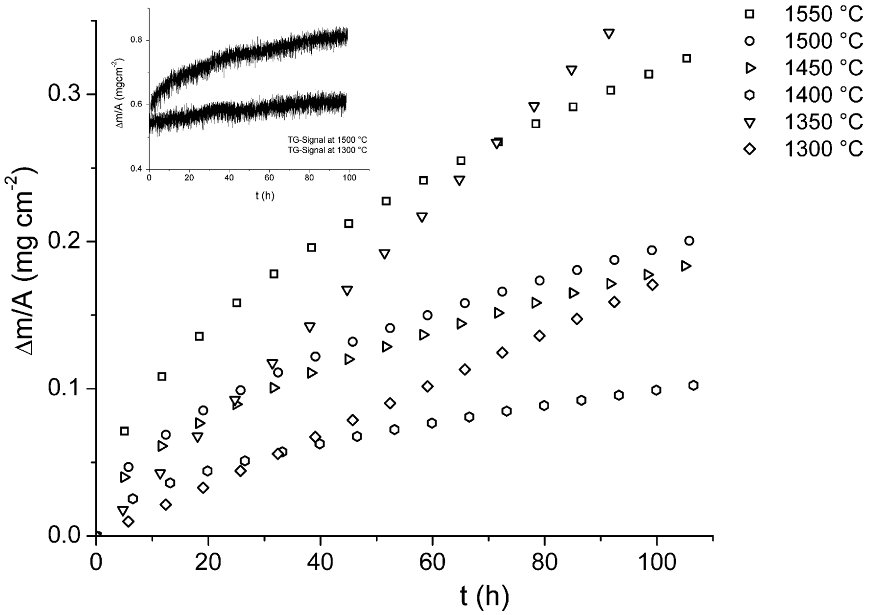

Fig. 5. Mass increase as a function of time of mullite coated C/C–SiC substrates in the temperature range 1300 °C ≤ T ≤ 1550 °C. The presented data are corrected for buoyancy and smoothed. In the insert, the raw data for samples at 1300 and 1500 °C are presented.

is too rapid to explain the experimentally observed growth rates. This comparison also sheds some light on how misleading it can be to compare only activation enthalpies (of parabolic rate constants and diffusivities) and to draw conclusions from (obviously) fortuitous numerical similarities. For our calculations we took the experimental data on oxygen diffusion in vitreous silica and in β-cristobalite from the work by Rodriguez-Viejo et al.,[27] as their data yield the least (though still too large) discrepancies with our experimental rate constants, as compared to data taken from other sources.

Likewise, the linear growth rate cannot be explained by oxygen transport in mullite, as can be seen from Table 3: oxygen transport is, again, too rapid. Case A has thus to be discarded.

In case B transport of CO in silica and mullite is assumed to be the rate determining step. Because of the lack of diffusivity data and solubility values of CO in the two oxide matrices it is impossible, as yet, to come to an unambiguous conclusion. But it is difficult to imagine another species rather than CO to control the reaction rate, once oxygen had to be discarded. A further, though weak, argument in sup-

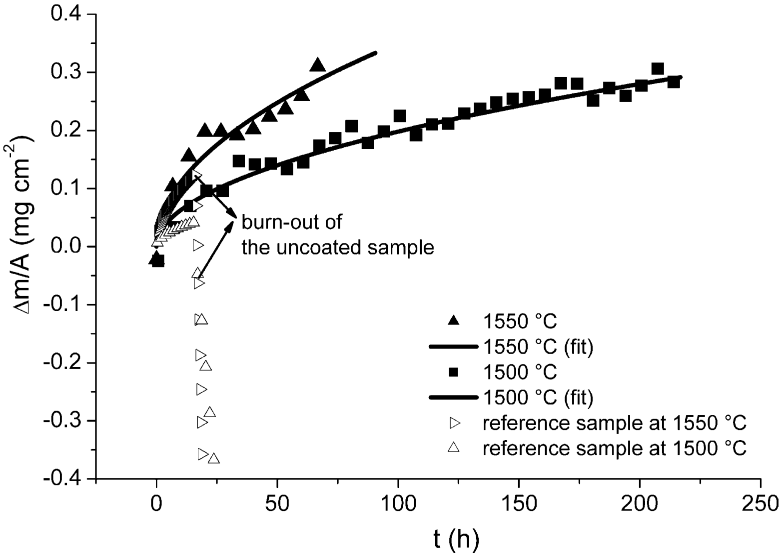

Fig. 6. Raw data for the mass increase of reference samples (open symbols) and mullite coated C/C–SiC substrates at 15 V cm^{-1} for 15 s (full symbols). The solid curves are parabolic fits of the experimental data.

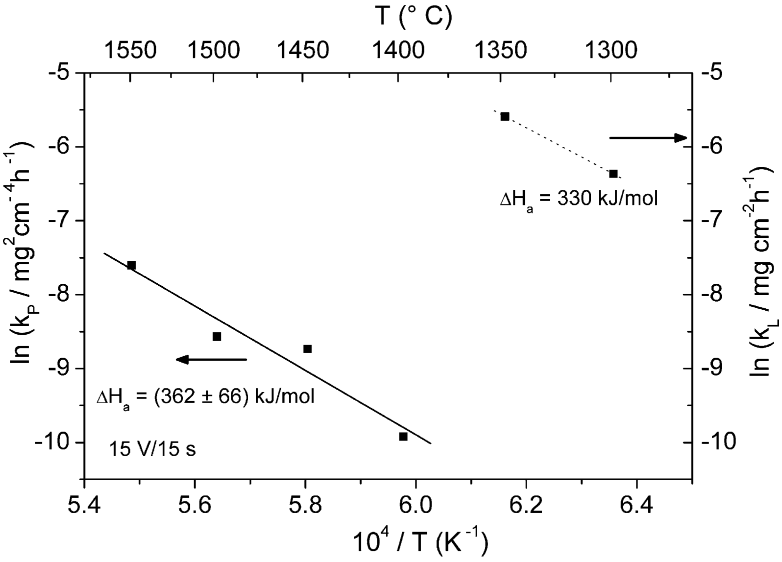

Fig. 7. Linear rate constant, k'_L, and parabolic rate constant, k'_P, respectively, for the temperature ranges 1300 °C ≤ T ≤ 1350 °C and 1400 °C ≤ T ≤ 1550 °C.

port of the role of CO can be drawn from the fact that the permeation parameters (Dc) of CO in silica and mullite do not differ dramatically.

The raw data of the TG analysis for two mullite coated samples (with a parabolic fit for each sample) and the raw data for unprotected C/C–SiC reference samples are shown in Fig. 6 for two different temperatures. From Fig. 6 it is obvious that unprotected C/C–SiC reference samples exhibit a rapid mass loss due to the burn-out of the carbon composite after about 20 h of oxidation.

7. Conclusions

From our results the following conclusions can be drawn:

- The combination of sol–gel technology and electrophoretic deposition allows to obtain mullite coatings which are suitable for prolonged isothermal applications under oxidizing conditions in the temperature range from 1300 to 1550 °C.
- The mass increase of the coated samples results from the passive oxidation of the SiC layer.
- The oxidation rate of the mullite coated material is significantly reduced as compared to uncoated C/C–SiC reference material.
- At lower temperatures or short times of oxidation the overall oxidation kinetics are determined by the transport processes in the EPD mullite layer, which leads to a linear growth law.
- At higher temperatures or longer times of oxidation the oxidation rate is controlled by solid state diffusion processes in the growing silica layer, which leads to a parabolic growth law.
- The complex growth law can be rationalized on the basis of a phenomenological model.
- Comparison of experimental parabolic and linear rate constants with calculated ones leads, in the framework of the model, to the conclusion that carbon monoxide (CO) diffusion in the oxide layers is the rate determining step, rather than oxygen diffusion (which would be too rapid).

Acknowledgements

We are indebted to Mr. E. Ebeling for the sample preparation. Financial support of the Deutsche Forschungsgemeinschaft (DFG) and of the Deutsche Akademische Austausch Dienst (DAAD) made this work possible. The most valuable comments of two anonymous reviewers helped to improve the manuscript.

References

1. Fritze, H., Jojić, J., Witke, T., Rüscher, C., Weber, S., Scherrer, S. *et al.*, Mullite based oxidation protection for SiC–C/C composites in air at temperatures up to 1900 K. *J. Eur. Ceram. Soc.* 1998, **18**, 2351–2364.
2. Schneider, H., Okada, K. and Pask, J. A., *Mullite and Mullite Ceramics*. John Wiley and Sons, Chichester, 1994, pp. 1–125.
3. Lee, K. N., Jacobson, N. S. and Miller, R. A., Refractory oxides on SiC ceramics. *MRS Bull.* 1994, **19**, 35–38.
4. Lee, K. N. and Miller, R. A., Oxidation behavior of mullite coated SiC and SiC/SiC composites under thermal cycling between room temperature and 1200–1400 °C. *J. Am. Ceram. Soc.* 1996, **79**, 620–626.
5. Fielitz, P., Borchardt, G., Schneider, H., Schmücker, M., Wiedenbeck, M. and Rhede, D., Self-diffusion of oxygen in mullite. *J. Eur. Ceram. Soc.* 2001, **21**, 2577–2582.
6. Fielitz, P., Borchardt, G., Schmücker, M., Schneider, H. and Willich, P., Oxygen grain boundary diffusion in polycrystalline mullite ceramics. *J. Am. Ceram. Soc.* 2003, in press.
7. Jojić, J., *Elektrophoretisch und mittels sol–gel-Verfahren abgeschiedene Schichten auf Mullitbasis als Hochtemperaturoxidation-*

sschutz von C/C-Werkstoffen. Ph.D. thesis, Technische Universität Clausthal, Germany, 1999.

8. Lee, K. N., Miller, R. A. and Jacobson, N. S., New generation of plasma-sprayed mullite coatings on silicon-carbide. *J. Am. Ceram. Soc.* 1995, **78**, 705–710.
9. Yoldas, B., Mullite formation from aluminium and silicon alkoxides, in mullite and mullite matrix composites. In *Ceramic Transactions, Vol 6*, ed. S. Somiya, R. F. Davis and J. A. Pask. American Ceramic Society, Westerville, OH, 1990, p. 255.
10. Livage, J. and Sanchez, C., Sol–gel chemistry. *J. Non-Cryst. Solids* 1992, **145**, 11–19.
11. Brinker, C. J. and Scherer, G. W., *Sol–Gel Science: The Physic and Chemistry of Sol–Gel Processing*. Academic Press, San Diego, CA, 1990.
12. Colomban, P., Structure of oxide gels and glasses by infrared and Raman-scattering: 2. Mullites. *J. Mater. Sci.* 1989, **24**, 3011–3020.
13. Yoldas, B. E. and Partlow, D. P., Formation of mullite and other alumina-based ceramics via hydrolytic polycondensation of alkoxides and resultant ultra- and micro-structural effects. *J. Mater. Sci.* 1988, **23**, 1895–1900.
14. Sanchez, C., Livage, J., Henry, M. and Babonneau, F., Chemical modification of alkoxide precursors. *J. Non-Cryst. Solids* 1988, **100**, 65–76.
15. Heinrich, T. and Raether, F., Structural characterization and phase development of sol–gel-derived mullite and its precursors. *J. Non-Cryst. Solids* 1992, **147–148**, 152–156.
16. Schneider, H., Merwin, L. and Sebald, A. J., Mullite formation from non-crystalline precursors. *J. Mater. Sci.* 1992, **27**, 805–812.
17. Rehak, P., *Untersuchung der Hydrolyse, der Precursorstadien und der Struktur von Sol–gel präparierten Mulliten mittels NMR*. Ph.D. thesis, F.-Schiller-Universität, Jena, Germany, 1996.
18. Bodart, P. R., Parmentier, J., Harris, R. K. and Thompson, D., Aluminium environments in mullite and an amorphous sol–gel precursor examined by ^{27}Al triple-quantum MAS NMR. *J. Phys. Chem. Solids* 1999, **60**, 223–228.
19. Schmücker, M. and Schneider, H., A new approach on the coordination of Al in non-crystalline gels and glasses of the system Al_2O_3–SiO_2. *Ber. Bunsenges. Phys. Chem.* 1996, **100**, 1150–1553.
20. Taylor, A. and Holland, D., The chemical synthesis and crystallization sequence of mullite. *J. Non-Cryst. Solids* 1993, **152**, 1–17.
21. Jaymes, I., Douy, A., Massiot, D. and Coutures, J. P., Characterization of mono and diphasic mullite precursor powders prepared by aqueous routes ^{27}Al and ^{29}Si MAS-NMR spectroscopy investigations. *J. Mater. Sci.* 1996, **31**, 4581–4589.
22. Smith, M. E., Application of ^{27}Al NMR techniques to structure determination in solids. *Appl. Magn. Reson.* 1993, **4**, 1–64.
23. Sarkar, P. and Nicholson, P. S., Electrophoretic deposition (EPD): mechanisms, kinetics and application to ceramics. *J. Am. Ceram. Soc.* 1996, **79**, 1987–2002.
24. Van der Biest, O. O. and Vandeperre, L. J., Electrophoretic deposition of materials. *Annu. Rev. Mater. Sci.* 1999, **29**, 327–352.
25. Alpha-Step 500, Surface Profiler, User Manual.
26. Fielitz, P., Borchardt, G., Schmücker, M., Schneider, H. and Willich, P., Measurement of oxygen grain boundary diffusion in mullite ceramics by SIMS depth profiling. *App. Surf. Sci.* 2003, **203**, 639–643.
27. Rodriguez-Viejo, J., Sibieude, F. and Clavaguera-Mora, M. T., High-temperature oxidation of CVD Beta-SiC 2. Relation between oxygen diffusion-coefficients and parabolic rate constants. *J. Eur. Ceram. Soc.* 1994, **13**, 177–184.
28. Barin, I., *Thermochemical Data of Pure Substances*. VCH Verlagsgesellschaft mbH, Weinheim.
29. Luthra, K. L., Some new perspectives in oxidation of silicon carbide and silicon nitride. *J. Am. Ceram. Soc.* 1991, **74**, 1095–1103.
30. Luthra, K. L., Theoretical aspects of the oxidation of silica-forming ceramics. In *Corrosion of Advanced Ceramics: Measurement and Modelling, Vol 267, Series E: Applied Sciences*, ed. K. G. Nickel. Kluwer Academic Publishers, 1994, pp. 23–34.
31. Luthra, K. L., Oxidation of carbon/carbon composites—a theoretical analysis. *Carbon* 1988, **26**, 217–224.